RSC Advances

PAPER

View Article Online
View Journal | View Issue

Cite this: *RSC Adv.*, 2019, **9**, 42343

Enhancing the adsorption capability of areca leaf biochar for methylene blue by K_2FeO_4-catalyzed oxidative pyrolysis at low temperature

Zhibing Yin,[ab] Nian Liu,[ab] Siyao Bian,[ab] Jihui Li,[*ab] Shuying Xu[*ab] and Yucang Zhang[ab]

Received 22nd August 2019
Accepted 9th December 2019

DOI: 10.1039/c9ra06592j

rsc.li/rsc-advances

Catalytic oxidative pyrolysis is a promising method for the preparation of highly adsorptive biochar by introducing oxygen-containing groups. Here, a K_2FeO_4-catalyzed oxidative pyrolysis was described for enhancing the adsorption capability of areca leaf biochar toward methylene blue at low temperature. It was shown that the maximum adsorption capacity of the biochar pyrolyzed at 200 °C was greatly improved from 122.67 to 251.95 mg g^{-1} with the catalysis of K_2FeO_4 due to the introduction of surface oxygen-containing groups. In addition, a high adsorption capability was observed over a wide pH range for the K_2FeO_4-modified biochar and nearly neutral pH was obtained after adsorption, further demonstrating the great advantages of K_2FeO_4-catalyzed oxidative pyrolysis. Mechanistic studies revealed that the adsorption of the pristine biochar was mainly determined by hydrogen bonding and electrostatic interaction. Whereas, the adsorption of the K_2FeO_4-modified biochar was attributed to cation exchange besides hydrogen bonding and electrostatic interactions.

1. Introduction

Biochar, a carbon-rich material made by thermal conversion of biomass under limited oxygen atmosphere, has attracted increasing attention as a green and low-cost adsorbent for environmental remediation.[1–3] Generally, pristine biochar can be easily prepared by conventional pyrolysis, gasification, torrefaction and hydrothermal carbonization,[4–7] but suffered from low adsorption capability.[8] For expanding the application of biochar, acid, alkaline, oxidation and mineral-impregnation modifications have been developed for improving the adsorption capability of biochar in the past decay.[9–12] However, excessive chemicals are usually employed,[9] causing potential pollution during preparation. Moreover, relatively high pyrolysis temperature is required, causing high energy consumption and loss of functional groups which play an important role in adsorption.[13] Thus, green modification with low pyrolysis temperature is highly pursued for enhancing the adsorption capability of biochar.

Catalytic pyrolysis, an efficient technology for accelerating carbonization of biomass using a catalytic amount of promoter,[14] can be a green method for preparation of biochar. However, it is a challenge to make highly adsorptive biochar *via* catalytic pyrolysis as easily causing loss of surface functional groups even at low temperature. Comparing with other catalytic pyrolysis, catalytic oxidative pyrolysis can produce additional oxygen-containing groups, thereby cover the shortage of functional group decrease. Anyhow, it is of vital importance to find out a highly active catalyst for the preparation of highly adsorptive biochar. An efficient oxidation catalyst can promote oxidative carbonization of biomass to generate surface functional group-rich biochar at low temperature. To the best of our knowledge, no catalytic oxidative pyrolysis has been developed for improving the adsorption capability of biochar by now.

Methylene blue (MB), a common toxic and coloured pollutant, is widely present in wastewater discarded from printing, paper and textile industries.[15,16] MB can be persisted for a long time even exposure to light and water, causing serious threat not only to human health but also to environment.[17–19] Great advance has been made for removal of MB using biochar as adsorbent over the past decade.[6,16,17] Especially, the $ZnCl_2$,[20] H_2O_2 [21,22] and NaOH-engineered[23] biochars were prepared for removal of MB from aqueous solution due to their relatively high adsorption capabilities. Yet, largely excessive modifier and high pyrolysis temperature are required for the preparation of these biochars.

Here, a K_2FeO_4-catalyzed oxidative pyrolysis was explored for the preparation of highly adsorptive areca leaf biochar for removal of MB from aqueous solution. Being a strong oxidant, K_2FeO_4 should effectively catalyze oxidative carbonization of biomass to generate oxygen-containing group-rich biochar at

[a]*Key Laboratory of Ministry of Education for Advanced Materials in Tropical Island Resources, College of Materials and Chemical Engineering, Hainan University, Haikou 570228, China. E-mail: lijihui@hainanu.edu.cn; xushuying1980@hainanu.edu.cn*

[b]*Hainan Provincial Key Lab of Fine Chem, College of Materials and Chemical Engineering, Hainan University, Haikou 570228, China*

low temperature. The targets of this study were to: (1) developed a green method for improving the adsorption capability of biochar, (2) evaluate the adsorption capability of the biochar toward MB in aqueous solution, (3) illuminate the adsorption mechanism.

2. Materials and methods

2.1 Materials

Areca leaves were obtained from Fengyu farm in Ledong county of Hainan province, China. The chemicals including HCl, KOH, MB and K_2FeO_4 were analytically pure reagents purchased from Aladdin and Macklin in Shanghai of China. A MB solution (1000 mg L^{-1}) was prepared by dissolving 1000 mg MB into 1 L deionized water, then diluted to the desired concentrations (25–350 mg L^{-1}). The pH of MB solution was adjusted by HCl or NaOH solution with suitable concentration.

2.2 Biochar preparation

The dried areca leaves were washed with water to remove impurities, dried in an oven at 60 °C for 24 h. The areca leaves were cut into small pieces, then pulverized and passed through a 60 mesh sieve to obtain a powder having a particle diameter of less than 2.5 mm. The areca leaf powder was pre-treated with K_2FeO_4 followed by pyrolysis to make modified biochar (MBC). Briefly, 0.5 g K_2FeO_4 was quickly dissolved in 100 mL of deionized water, then 5 g areca leaf powder was added to the aqueous solution, sonicated in an ultrasonic cleaner for 120 minutes and dried in an oven at 60 °C. The pre-treated areca leaf powder was pyrolyzed at different temperatures in a vacuum tube furnace under nitrogen with a heating rate of 5 °C min^{-1}, kept at the targeted temperature for 1 h. The pyrolyzed product was washed with deionized water until colourless, dried in an oven at 60 °C for 24 h to obtain the MBC. Correspondingly, the pristine biochar (PBC) was directly prepared from areca leaf powder without K_2FeO_4 treatment. According to pyrolysis temperature, the PBCs and MBCs were named PBC200, PBC300, PBC400, PBC500, PBC600 and MBC200, MBC300, MBC400, MBC500, MBC600, respectively. Additionally, the MBCs pyrolyzed at 200 °C with 1/20 and 1/5 mass ratios of K_2FeO_4 to biomass were labelled as MBC200-1 and MBC200-2, respectively.

2.3 Biochar characterization

The physical parameters including the specific surface area (SSA), pore volume (PV), and pore diameter (PD) were determined by nitrogen gas sorption isotherm on a surface area and porosity analyzer (Micromeritics ASAP 2460, America). The SSA was calculated by Brunauer–Emmett–Teller (BET) method. The PV and PD were calculated by Barret–Joyner–Halenda (BJH) method.

Fourier transform infrared spectroscopy (FTIR) was applied to determine the functional groups of biochar. A certain amount of biochar (2 mg) and KBr (1000 mg) were mixed, ground and pressed into sheet, then recorded between 400 and 4000 cm^{-1} on a FTIR spectrometer (Bruker Tensor 27, Ettlingen, Germany). The surface functional group and element composition was characterized by an X-ray photoelectron spectrometer (XPS) (Thermo Scientific Escalab 250Xi, America).

The element content of biochar was measured on an organic element analyzer (Thermo Scientific Flash 2000 CHNS/O, America) and an inductive couple plasma (ICP) elemental analyzer (Agilent ICPOES 730, America). The possible crystalline of the biochar was examined on an X-ray diffractometer (Brucker D8 Advance, Germany).

2.4 Batch adsorption experiments

Generally, the adsorption experiments were carried out by mixing 20 mg areca leaf biochar and 40 mL MB solution into a 150 mL flask, then shaken in a constant temperature oscillator with 180 rpm speed for desired time. For investigating the effect of pyrolysis temperature, the adsorption was performed at 25 °C for 24 h using 100 mg L^{-1} MB concentration. The effect of initial pH was investigated in 150 mg L^{-1} MB solution over a range of pH from 3 to 9 for 24 h. The 1/8, 1/4, 1/2, 3/4, 4/4, 5/4 ratios of biochar to MB solution (mg mL^{-1}) were employed to study the effect of biochar dosage by performing the adsorption in 100 mg L^{-1} MB solution for 36 h. The kinetic adsorption experiments were investigated at 25 °C and pH 7 with different time intervals (0.25, 0.5, 1, 2, 4, 8, 12, 16, 24, 30, 36 and 48 h), 75, 100, 150 and 200 mg L^{-1} concentrations were tested. A series of concentrations (25, 50, 75, 100, 150, 200, 250, 300 and 350 mg L^{-1}) were applied for studying adsorption isotherms at pH 7 for 48 h, and the adsorption experiment was conducted at 15, 25, 35 and 45 °C, respectively. All the experiments were performed in triplicates.

The concentration of MB solution was measured on an UV-vis spectrophotometer (MAPADA UV-3300PC, Shanghai of China) at 665 nm. The adsorption capability was determined by the difference of MB concentrations before and after adsorption. The adsorption capabilities of PBC and MBC were calculated by the equation expressed as:

$$Q_t = (C_0 - C_t)V/M$$

Q_t (mg g^{-1}) is the adsorption capability of biochar; C_0 (mg L^{-1}) and C_t (mg L^{-1}) are the concentrations of MB solution at adsorption time 0 and t, respectively; V (L) is the volume of MB solution; M (g) is the weight of PBC and MBC.

3. Results and discussion

3.1 Biochar characterization

As shown in Table 1, both pristine and modified biochars were of mesoporous as other ones.[24] The SSA of pristine biochar increased as the pyrolysis temperature increased from 200 to 500 °C, and sharply decreased while rose to 600 °C. For the modified biochar, the SSA always increased with pyrolysis temperature. It was noted that both PBC200 and MBC200 were poor of SSA and PV. Thus, these properties contributed less to the adsorption capacities of PBC200 and MBC200.

The total element composition of biochar was presented in Table 2. The pristine biochar was mainly comprised of C, O, N

Table 1 Physical characteristics of biochar

BC	SSA (m^2 g^{-1})	PV (cm^3 g^{-1})	PD (nm)
PBC200	0.62	0.0022	11.69
PBC300	2.15	0.0103	16.86
PBC400	6.45	0.0177	10.25
PBC500	42.98	0.0229	4.03
PBC600	1.16	0.0156	41.53
MBC200	0.66	0.0033	17.41
MBC300	1.28	0.0070	18.44
MBC400	5.23	0.0121	16.01
MBC500	5.43	0.0127	29.79
MBC600	79.29	0.0234	9.93

Table 2 Element composition of biochar

	Organic elemental compositions (wt%)						ICP (wt%)	
Biochar	C	O	N	H	O/C[a]	N/C[a]	Fe	K
PBC200	47.87	35.83	1.43	5.89	0.56	0.026	0.02	0.01
PBC300	55.06	21.68	1.63	4.73	0.30	0.025	0.03	0.49
PBC400	55.88	15.51	1.75	3.71	0.21	0.027	0.04	0.75
PBC500	60.17	10.66	1.63	3.22	0.13	0.023	0.06	1.03
PBC600	68.01	8.56	1.88	2.64	0.09	0.024	0.09	0.65
MBC200	43.36	33.95	1.27	5.59	0.59	0.025	5.40	1.41
MBC300	47.45	27.46	1.61	4.32	0.43	0.029	8.36	1.45
MBC400	48.63	23.57	1.40	3.68	0.36	0.025	8.16	2.94
MBC500	47.90	20.96	1.23	2.46	0.33	0.022	9.53	3.40
MBC600	50.96	19.40	1.18	2.48	0.29	0.020	10.21	3.13

[a] Mol ratio.

and H with small amount of Fe and K. The modified biochar had similar elements with PBC200, but owned much more iron and potassium which could be derived from K_2FeO_4. The O content of both biochars decreased with increasing pyrolysis temperature as expected. Importantly, the O/C ratio of the modified biochar was usually higher than that of the pristine biochar, so new oxygen containing groups were introduced through K_2FeO_4 oxidation. N/C ratio of MBC200 was comparable to PBC200, suggesting nitrogen-containing groups could survive with K_2FeO_4 catalysis.

The FTIR spectra of biochars pyrolyzed at different temperatures were shown in Fig. 1. The broad peaks at approximately 3446 cm^{-1} were assigned to –OH stretching vibrations. The

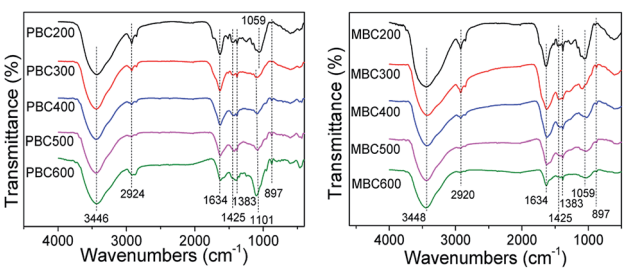

Fig. 1 FTIR spectral of biochar.

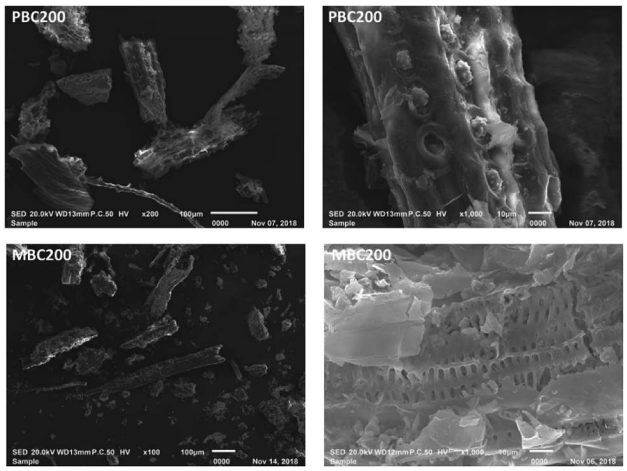

Fig. 2 SEM images of PBC200 and MBC200.

peaks around 2924 cm^{-1} belonged to aliphatic C–H stretching vibrations.[25,26] The peaks at 1634 cm^{-1} attributed to C=O and aromatic C=C stretching vibrations.[27] The adjacent peaks at about 1425 cm^{-1} were also assigned to aromatic C=C stretching vibrations. The peaks around 1383 cm^{-1} represented –COOH asymmetric bending vibrations.[28] The peaks around 1101 and 1059 cm^{-1} corresponded to aromatic and aliphatic C–O stretching vibrations, respectively. The peaks at 897 cm^{-1} represented aromatic C–H bending vibrations.[29]

The pristine biochar was mainly consisted of OH, COOH, C=O, C=C, C–O and aliphatic C–H groups as prepared at low temperature (≦400 °C). As previous reports,[30,31] the C=O peaks decreased and aromatic structure formed while higher temperature was applied. Interestingly, the pristine biochar prepared at 500 and 600 °C was still rich of C–O groups as C–O peaks (1101 cm^{-1}) became stronger. This was opposed to other reports.[31–33] Comparing to the corresponding pristine biochar, the modified biochar was much richer in aliphatic C–O and COOH groups as pyrolyzed at 200 °C. The aliphatic C–O groups of modified biochar decreased but no aromatic rings formed while increasing pyrolysis temperature. Moreover, strong peaks of C=O around 1634 cm^{-1} were always observed for the modified biochar. This demonstrated that K_2FeO_4 catalyzed pyrolysis could generate oxygen containing groups. As a result, K_2FeO_4 catalysis was beneficial to preparing oxygen containing group-rich biochar at low temperature.

The morphology of PBC200 and MBC200 was shown in Fig. 2. PBC200 was consisted of inhomogenous microparticles of which the surface was embedded with nbeans in row. With catalysis of K_2FeO_4, smaller microparticles with flocculences and micropores were obtained for MBC200. Therefore, K_2FeO_4 could efficiently accelerate the decomposition of areca leaf, which was helpful for making thermostable biochar at low pyrolysis temperature.

XPS spectra showed that the surface oxygen of MBC200 was much more than that of PBC200 due to K_2FeO_4 oxidation (Fig. 3). Whereas, only trace amount of iron was detected on the surface of MBC200, thereby iron was mostly embedded

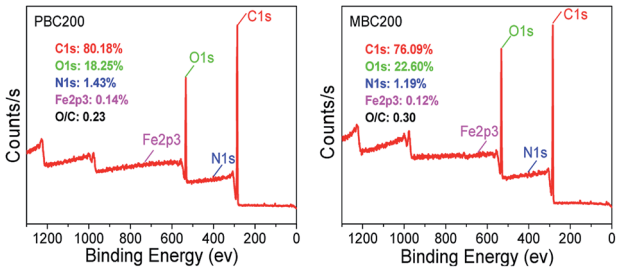

Fig. 3 XPS spectra of PBC200 and MBC200.

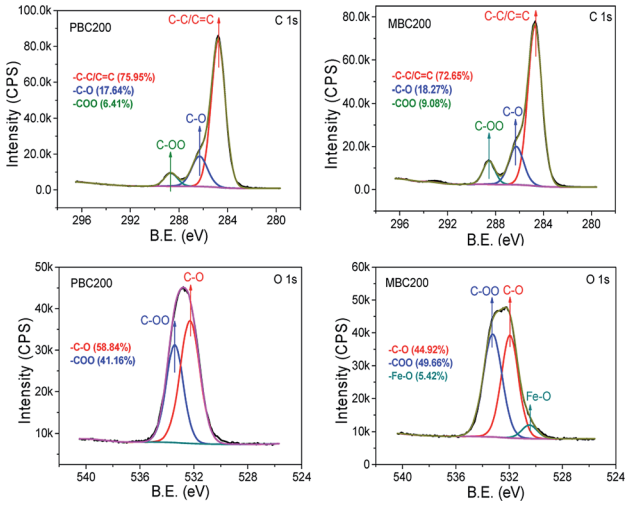

Fig. 4 C 1s and O 1s spectra of PBC200 and MBC200.

inside MBC200. The C 1s and O 1s spectra and their deconvolution results were shown in Fig. 4. The peaks centered at 284.8, 286.3 and 288.6 eV represented C–C, C–O and –CO_2– groups,[34,35] respectively. Both biochars were consisted of C–C/C=C, C–O and –CO_2– groups. Obviously, both C–O and –CO_2– groups of MBC200 were higher than that of PBC200, indicating new oxygen-containing groups were generated onto the surface of MBC200 with K_2FeO_4 oxidation. Moreover, a new peak at 530.5 eV, which could be assigned to Fe–O groups,[36,37] was observed on MBC200, indicating iron oxides were introduced.

The XRD patterns showed that a sharp diffraction peak at 21.38° and a broad diffraction peak between 8.30° and 27.02°

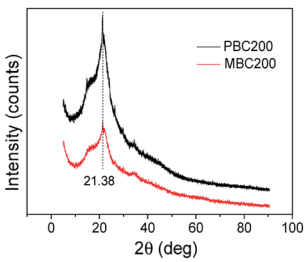

Fig. 5 XRD spectra of PBC200 and MBC200.

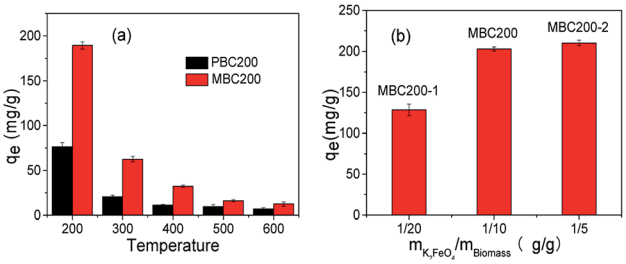

Fig. 6 Effect of pyrolysis temperature (a) and K_2FeO_4 amount (b) [20 mg biochar, 40 mL MB solution ((a) 100 mg L^{-1}, (b) 200 mg L^{-1}), pH = 7, 25 °C, 180 rpm, 24 h]. The error bars represented the standard deviation of triplicates.

(Fig. 5) were obtained for both PBC200 and MBC200. The peak around 21.38° could be attributed to well crystalline aliphatic carbon.[38] The broad peaks represented (110) and (200) planes of cellulose I.[39,40] The diffraction peak intensity of MBC200 was much weaker than that of PBC200 due to the oxidation of K_2FeO_4. No diffraction peaks of magnetic iron oxides such as Fe_3O_4 and γ-Fe_2O_3 were observed for MBC200, so no magnetism was obtained.

3.2 Adsorption behaviours toward MB

3.2.1 Effect of preparation parameters on adsorption capability. Pyrolysis temperature, a vital preparation parameter determining the physicochemical properties of biochar, significantly affected adsorption capability.[41] As seen in Fig. 6a, the adsorption capabilities of pristine and modified biochars toward methylene blue sharply decreased as the pyrolysis temperature increased from 200 to 300 °C. While further increasing pyrolysis temperature, the adsorption capabilities tardily decreased. Hence, the optimal pyrolysis temperature was 200 °C. The adsorption capability of modified biochar was always better than that of pristine one pyrolyzed at the same temperature. It was worthy to note that the adsorption capability of the biochar prepared at 200 °C was greatly raised from 76.62 to 189.32 mg g^{-1} with K_2FeO_4 modification. This could be ascribed to the introduction of additional oxygen-containing groups.

The dosage of K_2FeO_4 was also investigated (Fig. 6b). It was found that the adsorption capability remarkably increased as enhancing the weight ratio of K_2FeO_4 to biomass from 1/20 to 1/10, and rarely increased as further rising the dosage to 1/5. Anyway, these modifications all leaded to the increase of adsorption capability, demonstrating that the improvement of adsorption capability could be realized by using catalytic amount of K_2FeO_4. Considering both adsorption efficiency and K_2FeO_4 dosage, PBC200 and MBC200 were applied for studying their adsorption behaviours in the following experiments.

3.2.2 Effect of adsorption parameters on adsorption capability. As a crucial factor influencing the ion state of MB[42] and surface functional groups of biochar,[43] solution pH played an important role in adsorption of MB. The adsorption capability of PBC200 gradually increased with initial pH (Fig. 7a). For

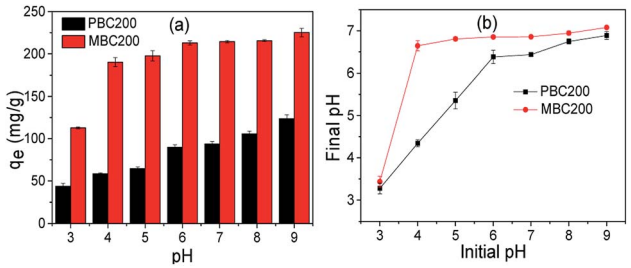

Fig. 7 Effect of solution pH (a) and pH variation after adsorption (b) [20 mg biochar, 40 mL MB solution (150 mg L^{-1}), pH = 7, 25 °C, 180 rpm, 24 h]. The error bars represented the standard deviation of triplicates.

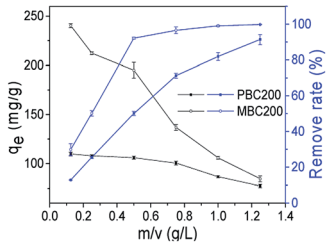

Fig. 8 Effect of biochar dosage (100 mg L^{-1} MB solution, pH = 7, 25 °C, 180 rpm, 36 h). The error bars represented the standard deviation of triplicates.

MBC200, the adsorption capability greatly increased from 112.86 to 190.10 mg g^{-1} as the initial pH was raised from 3 to 4, and almost maintained at this level while further increasing pH.

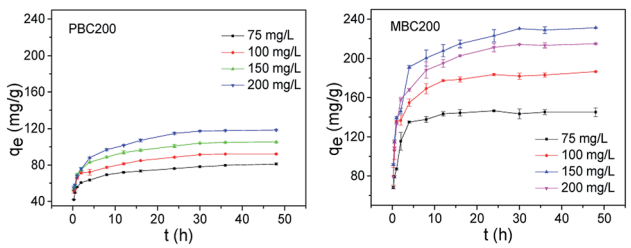

Fig. 9 Adsorption kinetics (20 mg biochar, 40 mL MB solution, pH = 7, 25 °C, 180 rpm). The error bars represented the standard deviation of triplicates.

This indicated that high adsorption capability was obtained for MBC200 over a wide pH range. Moreover, MBC200 always exhibited higher adsorption capability than PBC200 at the same initial pH.

The change of pH was recorded after adsorption (Fig. 7b). For PBC200, the pH slightly increased as the adsorption was performed between pH 3 and pH 6, and almost kept constant at about 7 while carried out beyond pH 6. For MBC200, the pH increased a little as pH 3 was applied and almost maintained around 7 when the adsorption was performed above pH 3.

The effect of biochar dosage was also investigated (Fig. 8). The removal rate of MB by PBC200 gradually increased as enhancing the dosage from 0.125 to 1.25 g L^{-1}. Removing 90% of MB required 1.25 g L^{-1} PBC200. For MBC200, the removal rate of MB rapidly increased up to 92.16% with the increase of dosage from 0.125 to 0.5 g L^{-1}, and slightly rose as further increasing the dosage. This also demonstrated that MBC200 surpassed PBC200 for removing MB from aqueous solution.

3.2.3 Adsorption kinetics. The adsorption kinetics was depicted in Fig. 9. The adsorption of MB by PBC200 increased with adsorption time and reached equilibrium after 30 h. The removal of MB by MBC200 quickly increased during initial 5 h, then gradually slowed down and finally reached equilibrium after 30 h. The equilibrium adsorption capability of MBC200 was more than two times higher than that of PBC200. Thus, K_2FeO_4-catalyzed modification resulted in the improvement of adsorption rate for MB.

The adsorption kinetic data was matched by pseudo-first-order and pseudo-second-order model (Table 3).[44] The adsorption kinetics of PBC200 and MBC200 were better fitted by pseudo-second-order model than pseudo-first-order model with extremely high determination coefficients. Moreover, the calculated equilibrium adsorption capabilities of pseudo-second-order model were much closer to the experimental results than that of pseudo-first-order model for both biochars. This suggested that the adsorptions should be chemisorption-controlled processes.[45]

3.2.4 Adsorption isotherms. The adsorption isotherms were investigated at different temperatures (Fig. 10). The adsorption capacity of PBC200 generally increased with initial concentration until reached maximum. MBC200 exhibited

Table 3 The fitted results of kinetic data

		Pseudo-first model: $\ln(q_e - q_t) = \ln q_e - k_1 t$				Pseudo-second model: $\frac{t}{q_t} = \frac{1}{k_2 q_e^2} + \frac{1}{q_e} t$			
BC	C_0 (mg L^{-1})	$q_{e,exp}$	$q_{e,cal}$	k_1	R^2	$q_{e,exp}$	$q_{e,cal}$	k_2	R^2
PBC200	75	81.06	27.97	0.079	0.96380	81.06	81.16	0.0134	0.99855
	100	92.14	41.22	0.136	0.92976	92.14	93.37	0.0118	0.99866
	150	105.27	46.53	0.121	0.96643	105.27	106.61	0.0098	0.99884
	200	118.46	63.08	0.128	0.98586	118.46	120.92	0.0068	0.99835
MBC200	75	146.38	29.44	0.187	0.68100	146.38	146.62	0.0169	0.99984
	100	186.54	54.28	0.215	0.84167	186.54	187.26	0.0085	0.99974
	150	214.70	93.92	0.309	0.94537	214.70	218.34	0.0052	0.99954
	200	231.17	103.21	0.283	0.90626	231.17	234.74	0.0044	0.99932

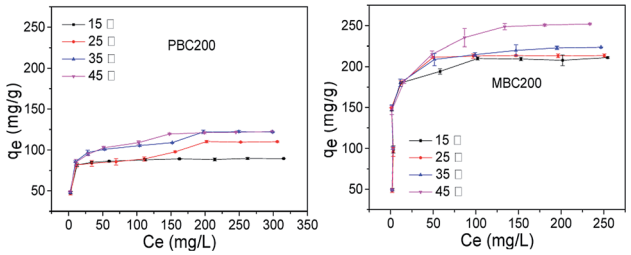

Fig. 10 Adsorption isotherms of PBC200 and MBC200 (20 mg biochar, 40 mL MB solution, pH = 7, 48 h, 180 rpm). The error bars represented the standard deviation of triplicates.

higher adsorption capacity than PBC200. The maximum adsorption capacities of both biochars slightly rose with adsorption temperature, implying these adsorptions were exothermic.

The adsorption isotherm data was simulated by Langmuir and Freundlich models (Table 4).[46] The adsorption processes of PBC200 and MBC200 were better described by Langmuir model than Freundlich model with extremely high correlation coefficients. In addition, the experimental maximum adsorption capacities approximated to the calculated results of Langmuir model. This indicated the removal of MB was a monolayer adsorption process.[15] It was noted that the adsorption capacity of MBC200 was superior or comparable to that of most adsorbents reported in the literature (Table 5).

3.2.5 Adsorption mechanism. As performing the adsorption of MBC200 at pH 4, the pH significantly rose after adsorption (Fig. 7b), indicating MBC200 had high cation exchange capability due to the generation of carboxylates (Fig. 4). Therefore, it could be concluded that cation exchange played an important role in the adsorption of MBC200. Instead, the pH change was not obvious after adsorption for PBC200, implying cation exchange less occurred. Thus, the introduction of new carboxylates contributed to the increase of adsorption capability with K_2FeO_4 modification.

As shown in Fig. 11, the C–N feature peaks of MB at 1398 and 1339 cm^{-1} shifted to 1385 and 1325 cm^{-1} as MB was adsorbed onto PBC200 and MBC200. Meanwhile, the COOH peaks of PBC200 and MBC200 around 1733 cm^{-1} almost disappeared after adsorption, probably attributing to the red shift of COOH peaks to lower wave-numbers which was overlapped by the peaks around 1628 cm^{-1}. Moreover, the COOH peaks appeared after desorption of MB in mixture of acetic acid/ethanol (1/9 volume ratio). These clearly demonstrated that hydrogen bonds were formed between MB and both biochars during adsorption.

As PBC200 and MBC200 were rich of surface oxygen containing groups, negatively charged surface might be generated under neutral conditions. Hence, the MB cation could be adsorbed onto the biochar surface by electrostatic interaction at pH 7.

Table 5 List of different adsorbents and their maximum adsorption capabilities (q_{max}) towards MB

Adsorbent	q_{max} (mg g^{-1})	Ref.
NaOH-activated carbon	890	47
$Ca(NO_3)_2$-activated carbon fiber	295	48
Carbon polyhedra	354	49
Magnetic chitosan/graphene oxide composite	180.83	50
Graphene oxide	598.8	51
Citric acid modified kenaf core fibre	131.6	52
Lotus leaf	221.7	53
Biochar/AlOOH nanocomposite	85.03	54
H_2O_2-assisted microwave activated biochar	91.0	21
K_2FeO_4-modified biochar	251.95	This work

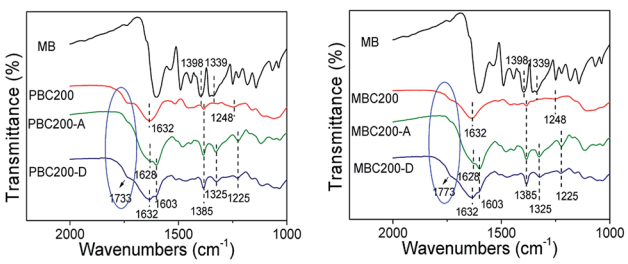

Fig. 11 FTIR spectra of biochars after adsorption and desorption. (PBC200-A or MBC200-A: biochar after adsorption; PBC200-D or MBC200-D: regenerated biochar).

Table 4 The fitted parameters of isotherm data

		Langmuir: $q_e = \frac{K_L q_{max} C_e}{1 + K_L C_e}$				Freundlich: $q_e = K_F C_e^{1/n}$		
BC	T (°C)	$q_{exp,max}$	$q_{cal,max}$	K_L	R^2	K_F	$1/n$	R^2
PBC200	15	89.66	90.09	0.444	0.99993	52.03	0.107	0.64727
	25	110.40	113.64	0.073	0.99073	45.41	0.158	0.85621
	35	122.57	125.15	0.102	0.99554	48.61	0.172	0.85968
	45	122.67	125.47	0.123	0.99877	49.43	0.173	0.90803
MBC200	15	211.05	213.22	0.279	0.99945	85.99	0.179	0.51464
	25	213.47	216.45	0.352	0.99957	87.13	0.183	0.50834
	35	223.71	226.75	0.259	0.99963	86.25	0.191	0.56792
	45	251.95	257.73	0.169	0.99904	81.84	0.226	0.66859

In brief, the adsorption of PBC200 could be mainly attributed to hydrogen bonding and electrostatic interaction. Differently, the adsorption of MBC200 involved cation exchange besides hydrogen bonding and electrostatic interaction.

4. Conclusions

A catalytic amount of K_2FeO_4 could effectively promote oxidative pyrolysis of areca leaf for preparation of highly adsorptive biochar for MB at 200 °C. The oxygen-containing groups were introduced onto the biochar through K_2FeO_4-catalyzed oxidative pyrolysis, where the functional groups of areca leaf were also mostly reserved. Therefore, the biochar displayed much higher adsorption capability than the pristine one. Moreover, high adsorption capability was observed over a wide pH range and nearly neutral pH was gained after adsorption. This will make the biochar serve as a promising adsorbent for remediation of MB-polluted wastewater in practice.

Conflicts of interest

There are no conflicts of interest to declare.

Acknowledgements

The Hainan Provincial Natural Science Foundation of China (519QN175) and the National Natural Science Foundation of China (21801053) were acknowledged.

Notes and references

1 F. R. Oliveira, A. K. Patel, D. P. Jaisi, S. Adhikari, H. Lu and S. K. Khanal, *Bioresour. Technol.*, 2017, **246**, 110–122.
2 T. Xie, K. R. Reddy, C. Wang, E. Yargicoglu and K. Spokas, *Crit. Rev. Environ. Sci. Technol.*, 2015, **45**, 939–969.
3 S. Ye, M. Yan, X. Tan, J. Liang, G. Zeng, H. Wu, B. Song, C. Zhou, Y. Yang and H. Wang, *Appl. Catal., B*, 2019, **250**, 78–88.
4 H. S. Kambo and A. Dutta, *Renewable Sustainable Energy Rev.*, 2015, **45**, 359–378.
5 L. Lonappan, T. Rouissi, R. K. Das, S. K. Brar, A. A. Ramirez, M. Verma, R. Y. Surampalli and J. R. Valero, *Waste Manag.*, 2016, **49**, 537–544.
6 L. Sun, S. Wan and W. Luo, *Bioresour. Technol.*, 2013, **140**, 406–413.
7 Y. Wang and R. Liu, *Fuel Process. Technol.*, 2017, **160**, 55–63.
8 S. J. Liu, Y. G. Liu, X. F. Tan, S. B. Liu, M. F. Li, N. Liu, Z. h. Yin, S. R. Tian and Y. H. Zhou, *J. Chem. Technol. Biotechnol.*, 2019, **94**, 2187–2197.
9 M. B. Ahmed, J. L. Zhou, H. H. Ngo, W. Guo and M. Chen, *Bioresour. Technol.*, 2016, **214**, 836–851.
10 T. Sizmur, T. Fresno, G. Akgul, H. Frost and E. Moreno-Jimenez, *Bioresour. Technol.*, 2017, **246**, 34–47.
11 X.-F. Tan, Y.-G. Liu, Y.-L. Gu, Y. Xu, G.-M. Zeng, X.-J. Hu, S.-B. Liu, X. Wang, S.-M. Liu and J. Li, *Bioresour. Technol.*, 2016, **212**, 318–333.
12 P. Zhang, S. Liu, X. Tan, Y. Liu, G. Zeng, Z. Yin, S. Ye and Z. Zeng, *Process Saf. Environ. Prot.*, 2019, **128**, 329–341.
13 P. Godlewska, H. P. Schmidt, Y. S. Ok and P. Oleszczuk, *Bioresour. Technol.*, 2017, **246**, 193–202.
14 G. Kabir and B. H. Hameed, *Renewable Sustainable Energy Rev.*, 2017, **70**, 945–967.
15 K. S. Tong, M. J. Kassim and A. Azraa, *Chem. Eng. J.*, 2011, **170**, 145–153.
16 M. T. Yagub, T. K. Sen, S. Afroze and H. M. Ang, *Adv. Colloid Interface Sci.*, 2014, **209**, 172–184.
17 M. S. Chiou and H. Y. Li, *Chemosphere*, 2003, **50**, 1095–1105.
18 E. N. El Qada, S. J. Allen and G. M. Walker, *Chem. Eng. J.*, 2006, **124**, 103–110.
19 Y. M. Slokar and A. M. L. Marechal, *Dyes Pigm.*, 1997, **37**, 335–356.
20 L. Shi, G. Zhang, D. Wei, T. Yan, X. Xue, S. Shi and Q. Wei, *J. Mol. Liq.*, 2014, **198**, 334–340.
21 V. Nair and R. Vinu, *Bioresour. Technol.*, 2016, **216**, 511–519.
22 D. V. Suriapparao, N. Pradeep and R. Vinu, *Energy Fuels*, 2015, **29**, 2571–2581.
23 X. Han, L. Chu, S. Liu, T. Chen, C. Ding, J. Yan, L. Cui and G. Quan, *BioResources*, 2015, **10**, 2836–2849.
24 Q. Chen, J. Zheng, L. Zheng, Z. Dang and L. Zhang, *Chem. Eng. J.*, 2018, **350**, 1000–1009.
25 S. Kumari, G. S. Chauhan and J. H. Ahn, *Chem. Eng. J.*, 2016, **304**, 728–736.
26 S. Liu, J. Li, S. Xu, M. Wang, Y. Zhang and X. Xue, *Bioresour. Technol.*, 2019, **282**, 48–55.
27 L. Qian and B. Chen, *J. Agric. Food Chem.*, 2014, **62**, 373–380.
28 F. Lian, B. Xing and L. Zhu, *J. Colloid Interface Sci.*, 2011, **360**, 725–730.
29 W. A. W. A. K. Ghani, A. Mohd, G. da Silva, R. T. Bachmann, Y. H. Taufiq-Yap, U. Rashid and A. a. H. Al-Muhtaseb, *Ind. Crops Prod.*, 2013, **44**, 18–24.
30 B. Chen and Z. Chen, *Chemosphere*, 2009, **76**, 127–133.
31 S. Xu, W. Yu, S. Liu, C. Xu, J. Li and Y. Zhang, *Sustainability*, 2018, **10**, 4250.
32 D. Chen, X. Yu, C. Song, X. Pang, J. Huang and Y. Li, *Bioresour. Technol.*, 2016, **218**, 1303–1306.
33 S. Duan, W. Ma, Y. Pan, F. Meng, S. Yu and L. Wu, *J. Taiwan Inst. Chem. Eng.*, 2017, **80**, 835–841.
34 H. Peng, P. Gao, G. Chu, B. Pan, J. Peng and B. Xing, *Environ. Pollut.*, 2017, **229**, 846–853.
35 P. Zhang, X. Tan, S. Liu, Y. Liu, G. Zeng, S. Ye, Z. Yin, X. Hu and N. Liu, *Chem. Eng. J.*, 2019, **378**, 122141.
36 T. Yamashita and P. Hayes, *J. Electron Spectrosc. Relat. Phenom.*, 2006, **152**, 6–11.
37 F. Yang, S. Zhang, H. Li, S. Li, K. Cheng, J.-S. Li and D. C. W. Tsang, *Chem. Eng. J.*, 2018, **348**, 191–201.
38 F. Yang, S. Zhang, Y. Sun, K. Cheng, J. Li and D. C. W. Tsang, *Bioresour. Technol.*, 2018, **265**, 490–497.
39 A. D. French, *Cellulose*, 2013, **21**, 885–896.
40 J. Miao, Y. Yu, Z. Jiang and L. Zhang, *Cellulose*, 2016, **23**, 1209–1219.
41 Y. Sun, B. Gao, Y. Yao, J. Fang, M. Zhang, Y. Zhou, H. Chen and L. Yang, *Chem. Eng. J.*, 2014, **240**, 574–578.

42 K. Sapana, S. C. Ghanshyam and A. Jou-Hyeon, *Chem. Eng. J.*, 2016, **304**, 728–736.
43 D. L. Guerra, H. C. P. Oliveira, P. C. C. da Costa, R. R. Viana and C. Airoldi, *Catena*, 2010, **82**, 35–44.
44 J.-P. Simonin, *Chem. Eng. J.*, 2016, **300**, 254–263.
45 M. K. Aroua, C. Y. Yin, F. N. Lim, W. L. Kan and W. M. Daud, *J. Hazard. Mater.*, 2009, **166**, 1526–1529.
46 P. K. Gessner and M. M. Hasan, *J. Pharm. Sci.*, 1987, **76**, 319–327.
47 A. M. M. Vargas, A. L. Cazetta, M. H. Kunita, T. L. Silva and V. C. Almeida, *Chem. Eng. J.*, 2011, **168**, 722–730.
48 S. Lei, J.-I. Miyamoto, H. Kanoh, Y. Nakahigashi and K. Kaneko, *Carbon*, 2006, **44**, 1884–1890.
49 J. Wang, C. Xue, Z. Wu, W. Li, Y. Lv, A. M. Asiri, B. Tu and D. Zhao, *Carbon*, 2012, **50**, 2546–2555.
50 L. Fan, C. Luo, M. Sun, X. Li, F. Lu and H. Qiu, *Bioresour. Technol.*, 2012, **114**, 703–706.
51 H. Yan, X. Tao, Z. Yang, K. Li, H. Yang, A. Li and R. Cheng, *J. Hazard. Mater.*, 2014, **268**, 191–198.
52 M. S. Sajab, C. H. Chia, S. Zakaria, S. M. Jani, M. K. Ayob, K. L. Chee, P. S. Khiew and W. S. Chiu, *Bioresour. Technol.*, 2011, **102**, 7237–7243.
53 X. Han, W. Wang and X. Ma, *Chem. Eng. J.*, 2011, **171**, 1–8.
54 M. Zhang and B. Gao, *Chem. Eng. J.*, 2013, **226**, 286–292.

